Identifiability and observability analysis for experimental design in nonlinear dynamical models

A. Raue,[1,2,a)] V. Becker,[3,b)] U. Klingmüller,[3,c)] and J. Timmer[1,4,d)]
[1]*Physics Institute, University of Freiburg, 79104 Freiburg, Germany*
[2]*Centre for Systems Biology (ZBSA), 79104 Freiburg, Germany*
[3]*Division of Systems Biology of Signal Transduction, DKFZ-ZMBH Alliance, German Cancer Research Center, 69120 Heidelberg, Germany and Bioquant, Heidelberg University, 69120 Heidelberg, Germany*
[4]*Freiburg Institute for Advanced Studies (FRIAS), 79104 Freiburg, Germany and Centre for Biological Signalling Studies (BIOSS), 79104 Freiburg, Germany*

(Received 30 September 2010; accepted 30 November 2010; published online 30 December 2010)

Dynamical models of cellular processes promise to yield new insights into the underlying systems and their biological interpretation. The processes are usually nonlinear, high dimensional, and time-resolved experimental data of the processes are sparse. Therefore, parameter estimation faces the challenges of structural and practical nonidentifiability. Nonidentifiability of parameters induces nonobservability of trajectories, reducing the predictive power of the model. We will discuss a generic approach for nonlinear models that allows for identifiability and observability analysis by means of a realistic example from systems biology. The results will be utilized to design new experiments that enhance model predictiveness, illustrating the iterative cycle between modeling and experimentation in systems biology. © *2010 American Institute of Physics*.
[doi:10.1063/1.3528102]

Ordinary differential equations are frequently used to investigate the dynamic properties of cellular processes such as signaling pathways. The aim is to match the mathematical model with the experimentally observed time-series data to reconstruct and validate the network structure and to predict system dynamics that is not accessible by experiments directly.[15] An important step is the estimation of beforehand unknown model parameters that determine the dynamical behavior. Intrinsically, the outcome of model predictions depends on the estimated model parameters and their *identifiability*. If model parameters are *nonidentifiable*, meaning that they are not well determined, some parts of the predicted model dynamics are also not, i.e., some components of the model may be *nonobservable*. Consequently, it might not be possible to infer the dynamical behavior of the system given the experimental data available. Inferring how identifiability and observability problems can be resolved by generating additional experimental data is the subject of *experimental design***.**

I. INTRODUCTION

In this article, we will introduce identifiability and its connection to observability and experimental design from a perception of parameter estimation. To this end, we discuss a generic approach that investigates identifiability by calculating the *profile likelihood*.[11] For illustration of the applicability of the approach, an illustrative case study utilizing an application[2] from cell biology is presented.

Assuming that diffusion is fast compared to the reaction rates of molecular interactions and the volume of the cell, cellular processes can be described by systems of ordinary differential equations (ODEs). The model equations

$$\dot{\vec{x}}(t,\theta) = \vec{f}(\vec{x}(t,\theta),\vec{u}(t),\theta), \tag{1}$$

$$\vec{y}(t_i,\theta) = \vec{g}(\vec{x}(t_i,\theta),\theta) + \vec{\epsilon}_i \tag{2}$$

describe, via the ODE system (1), the dynamics of n species $\vec{x}$ such as concentrations of proteins in different phosphorylation states. Their dynamical behavior may depend on an input function $\vec{u}(t)$, such as treatment with ligands, and model parameters $\theta=\{\theta_1,\ldots,\theta_l\}$, such as rate constants or species initial concentrations. Parameter values will be given on a $\log_{10}$ scale. The species $\vec{x}$ are mapped to m model observables $\vec{y}$, the quantities accessible by experiments at discrete times t_i, via an observation function $\vec{g}$ in Eq. (2). They may depend on additional parameters such as scaling or offset parameters included in θ. Often, only a subset or combinations of the modeled species are accessible by experiments, meaning that $m<n$. The distribution of the measurement noise $\epsilon_{ki}\sim N(0,\sigma_{ki}^2)$ is assumed to be known.

II. METHODS

Commonly, many model parameters θ are unknown and have to be estimated from experimental data. The agreement of experimental data $y_k^\dagger(t_i)$ with the observables predicted by the model $y_k(t_i,\theta)$ for parameters θ is measured by an

[a)]Electronic mail: andreas.raue@fdm.uni-freiburg.de.
[b)]Electronic mail: v.becker@dkfz-heidelberg.de.
[c)]Electronic mail: u.klingmueller@dkfz-heidelberg.de.
[d)]Electronic mail: jeti@fdm.uni-freiburg.de.

 © 2010 American Institute of Physics

Author complimentary copy. Redistribution subject to AIP license or copyright, see http://cha.aip.org/cha/copyright.jsp

objective function, commonly the weighted sum of squared residuals

$$\chi^2(\theta) = \sum_{k=1}^{m} \sum_{i=1}^{d_k} \frac{1}{\sigma_{ki}^2} (y_k^\dagger(t_i) - y_k(t_i, \theta))^2, \tag{3}$$

where d_k denotes the number of data points for each observable $k=1,\ldots,m$ measured at time points t_i with $i=1,\ldots,d_k$. The variances σ_{ki}^2 of the corresponding measurement errors are assumed to be known. The parameters can be estimated by finding the parameter values $\hat{\theta}$ that minimize $\chi^2(\theta)$. For normally distributed measurement noise, $\chi^2(\theta)$ is proportional to the log-likelihood and minimizing Eq. (3) corresponds to maximum likelihood estimation.[12] Therefore, $\chi^2(\theta)$ will be termed likelihood in the following.

The key point of our argument is that it is not sufficient to rely on the mere estimated parameter values and their corresponding prediction for the system dynamics. It is important to consider the uncertainties in the parameter estimation procedure: from measurement uncertainties, to parameter uncertainties and possibly nonidentifiabilities, to uncertainties in the predicted model dynamics and possibly nonobservabilities. Uncertainties in the parameter estimates are usually described by *confidence intervals*.[6] A confidence interval $[\sigma_i^-, \sigma_i^+]$ of a parameter estimate $\hat{\theta}_i$ to a confidence level $1-\alpha$ signifies that the true value θ_i^* is located within this interval with probability $1-\alpha$.

In order to evaluate the appropriateness of confidence intervals, usually, coverage rates are studied. The coverage rate (CR) for a parameter signifies how often its true value θ_i^* is actually covered by the confidence interval $[\sigma_i^-, \sigma_i^+]$. To this end, the data are simulated assuming a set of true parameter values. If confidence intervals are appropriate, the coverage rate should reflect the desired level of confidence $\mathrm{CR} \approx 1-\alpha$. If the coverage rate is larger than the desired level, the confidence intervals tend to be more conservative than required; if it is smaller, the actual uncertainty in the estimates is underestimated.

A. Identifiability

The parameter θ_i is *structurally identifiable* if its estimate $\hat{\theta}_i$ is a unique minimum of $\chi^2(\theta)$. It is *practically identifiable* if the confidence interval of its estimate has finite size. A nonidentifiable parameter indicates that it cannot be estimated from the experimental data, and hence its confidence intervals are infinite.

An approach for identifiability analysis utilizing the profile likelihood

$$\chi_{\mathrm{PL}}^2(\theta_i) = \min_{\theta_{j\neq i}} [\chi^2(\theta)] \tag{4}$$

was proposed by Raue *et al.*[11] The idea of the approach is to detect flatness of the likelihood by exploring the parameter space for each parameter in the direction of least increase in $\chi^2(\theta)$. Therefore, for each parameter θ_i, individually a section along the minimum of the objective function with respect to all of the other parameters $\theta_{j\neq i}$ is computed. At the same time, the profile likelihood enables to calculate *likelihood-based* confidence intervals.[9,16] Here, a threshold Δ_α in the likelihood defines a confidence region

$$\{\theta | \chi^2(\theta) - \chi^2(\hat{\theta}) < \Delta_\alpha\}, \tag{5}$$

whose borders represent confidence intervals.[8] The threshold Δ_α is the $1-\alpha$ quantile of the χ_{df}^2-distribution. The choice of df yields confidence intervals that hold jointly for df number of parameters.[10] Often, $df=1$ is applicable, yielding confidence intervals that hold individually for each parameter.

The difference $\chi^2(\theta^*) - \chi^2(\hat{\theta})$ corresponds to the amount of overfitting for the estimated parameters $\hat{\theta}$. For nonlinear models and small data samples, the actual distribution of $\chi^2(\theta^*) - \chi^2(\hat{\theta})$ may differ from the χ_{df}^2 distribution.[10] For instance, the distribution can be shifted if the actual degrees of freedom df consumed by the nonlinear model differs from the number of model parameters. Since the deviation of the distribution is dependent on the specific application, the distribution of $\chi^2(\theta^*) - \chi^2(\hat{\theta})$ should always be verified by simulation studies. If deviations are observed, the threshold Δ_α should be adjusted according to the generated distribution to obtain appropriate coverage rates for the confidence intervals.

Structural nonidentifiability. A structural nonidentifiability arises from the model structure only and is independent of the amount and quality of the given experimental data.[17] Assuming ideal measurements, with arbitrarily many and perfectly chosen measurement time points t_i and absence of measurements errors $\vec{\epsilon}_i=0$, the crucial question is whether the model parameters θ are uniquely estimable from the model observables $\vec{y}(t_i, \theta)$.

The formal analytical solution of $\vec{y}(t_i, \theta)$ may contain an ambiguous parametrization with respect to θ, arising from an insufficient mapping function $\vec{g}$ in Eq. (2) that is characterized by functional relations $\vec{h}(\theta_{\mathrm{sub}})=0$ of a subset of parameters $\theta_{\mathrm{sub}} \subset \theta$. In terms of likelihood, a structural nonidentifiability manifests as iso-χ^2 manifold

$$\{\theta | \vec{h}(\theta_{\mathrm{sub}}) = 0\} \Rightarrow \chi^2(\theta) = \mathrm{const.} \tag{6}$$

For a two-dimensional parameter space, a structural nonidentifiability can be visualized by a perfectly flat valley that is infinitely extended along the corresponding functional relation, as illustrated in Fig. 1(a). Correspondingly, this can be detected by a flat line of the profile likelihood for each parameter of θ_{sub} [see Fig. 1(b)]. Consequently, structural nonidentifiable parameters are not uniquely identified by measurements of $\vec{y}(t_i, \theta)$ and confidence intervals of $\theta_i \in \theta_{\mathrm{sub}}$ are infinite. A parameter is structurally identifiable if a unique minimum of $\chi^2(\theta)$ with respect to θ_i exists [see Figs. 1(c)–1(f)].

Practical nonidentifiability. A parameter that is structurally identifiable may still be practically nonidentifiable. This can arise due to insufficient amount and quality of experimental data or the chosen measurement time points. It manifests in a confidence interval that is infinite, although the likelihood has a unique minimum for this parameter.

A parameter is practically nonidentifiable if the likelihood-based confidence region (5) is infinitely extended in the direction of θ_i indicated by the likelihood staying be-

Author complimentary copy. Redistribution subject to AIP license or copyright, see http://cha.aip.org/cha/copyright.jsp

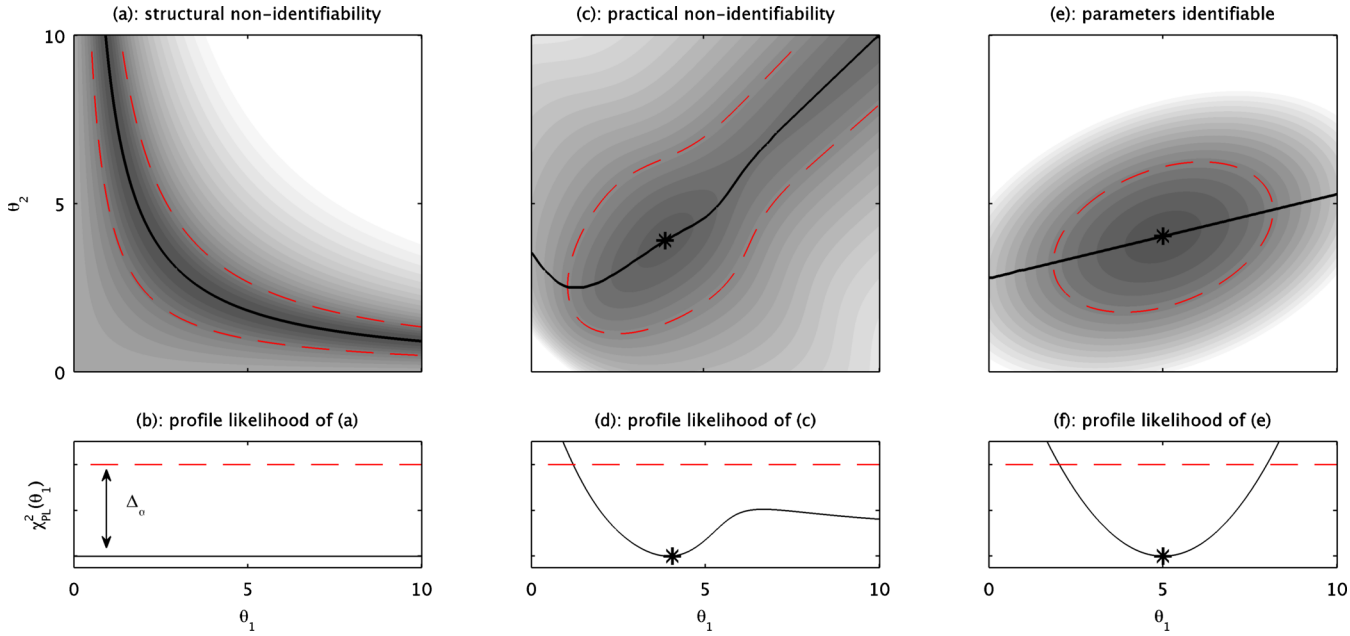

FIG. 1. (Color online) Assessing parameter identifiability of parameter θ_1 from the profile likelihood $\chi^2_{\mathrm{PL}}(\theta_1)$ indicated by the solid lines in (b), (d), and (f) and its corresponding trace in parameter space in (a), (c), and (e). Shades from black to white in (a), (c), and (e) correspond to low and high values of $\chi^2(\theta)$, respectively. The dashed lines indicate the threshold Δ_α utilized to assess likelihood-based confidence intervals and the asterisk corresponds to the optimal parameters $\hat{\theta}$ if available.

low a desired Δ_α.[11] Similar to structural nonidentifiability, the flattening out of the likelihood can continue along a functional relation. For a two-dimensional parameter space, a practical nonidentifiability can be visualized as a relatively flat valley, which is infinitely extended [see Fig. 1(c)]. This can be detected by the corresponding profile likelihood in Fig. 1(d), indicating that the height distance of the valley bottom to the lowest point at $\hat{\theta}$ never exceeds Δ_α. By increasing the amount and quality of the measured data and/or the choice of measurement time points t_i, stricter conditions on the parameter estimation are imposed. This leads to a tightening of confidence intervals that ultimately will remediate a practical nonidentifiability, yielding finite confidence intervals [see Figs. 1(e) and 1(f)].

B. Observability

The uncertainty in parameter estimates $\hat{\theta}$ indicated by nonidentifiability directly translates to uncertainty in model trajectories indicated by nonobservability. For structurally nonidentifiable parameters, those components of $\vec{x}$ affected by θ_{sub} can be nonobservable, whereas the model observables $\vec{y}$ are, by definition, invariant. In contrast, for practical nonidentifiable parameters, the model observables $\vec{y}$ are affected but stay in agreement with the uncertainties in the experimental data because the likelihood stays below the threshold Δ_α. Nevertheless, some components of $\vec{x}$ might be affected strongly by a practical nonidentifiability and hence might be nonobservable. Also, confidence intervals of parameter estimates translate to confidence intervals of model trajectories. Similar to coverage rates for confidence intervals of parameter estimates, coverage rates for confidence intervals of model trajectories can be assessed.

C. Experimental design

Since structural nonidentifiability is independent of the accuracy of experimental data, it cannot be resolved by increasing the amount and quality of the existing measurements. The only remedy is a qualitatively new measurement, which alters the mapping function $\vec{g}$ in Eq. (2), usually by increasing the number of the observed species. For practical nonidentifiability, increasing the amount and quality of the existing measurements may be sufficient but is often not very efficient.

To plan new experiments that efficiently resolve nonidentifiability problems, the set of trajectories along the profile likelihood of θ_i can be investigated.[11] This corresponds to the observability of the trajectories and reveals spots where the uncertainty in θ_i has the largest impact. Additional measurements at these spots promise to resolve both structural and practical nonidentifiabilities and narrow confidence intervals most efficiently. Furthermore, the amplitude of variability of the trajectories at these spots allows to assess the necessary measurement precision to provide adequate data.

III. APPLICATION

To demonstrate the usage of identifiability and observability analysis for experimental design, the profile likelihood approach will be applied to the core model of erythropoietin (Epo) and Epo receptor (EpoR) interaction and trafficking with the corresponding subset of the experimental data.[2] Briefly, in erythroid progenitor cells the dynamical properties of EpoR determine how signals encoded in the concentration of the ligand Epo are processed at the receptor level and how subsequently downstream signaling cascades such as the JAK2-STAT5 pathway are activated. This leads

Author complimentary copy. Redistribution subject to AIP license or copyright, see http://cha.aip.org/cha/copyright.jsp

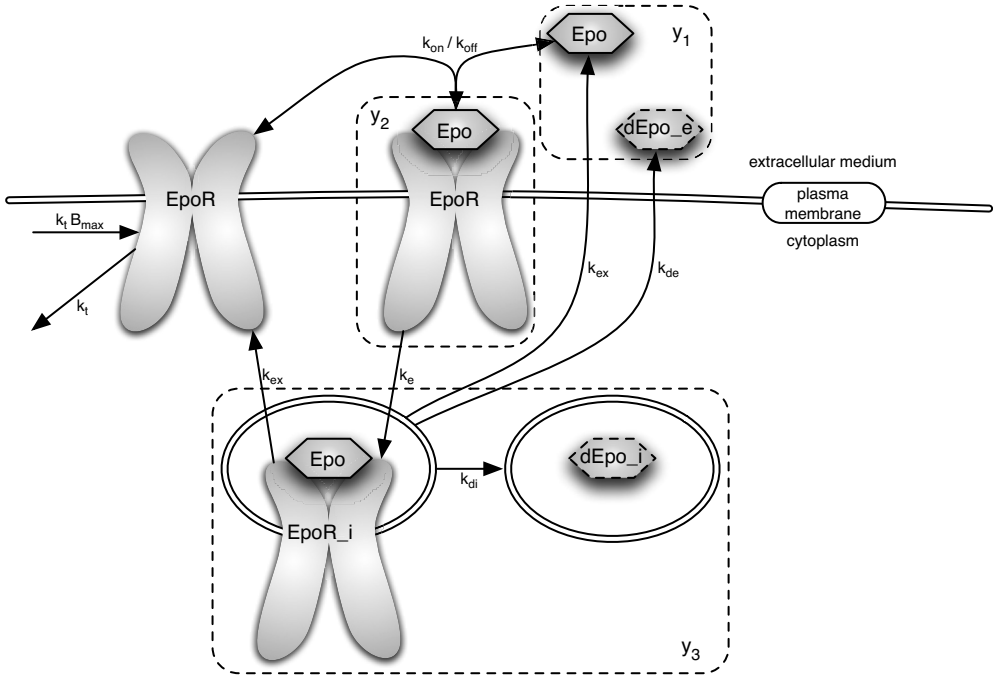

FIG. 2. Model for ligand binding as well as EpoR and ligand trafficking. The dashed boxes correspond to the quantities accessible by measurement of radioactively labeled ligand.

to cellular responses such as differentiation and proliferation of erythrocytes. A mathematical model is used to infer the dynamical characteristics of ligand binding and ligand as well as receptor trafficking because unoccupied EpoR is not directly accessible by experiments.

Model description. The central processes occurring at the EpoR level are depicted in Fig. 2. Six species are incorporated in the model: Epo, EpoR, Epo_EpoR complex, internalized complex Epo_EpoR_i, degraded internalized ligand dEpo_i, and degraded extracellular ligand dEpo_e. All interactions are modeled by mass-action kinetics. Briefly, Epo can bind to the extracellular domain of EpoR with association rate k_{on} [see v_1] and dissociates with rate $k_{\mathrm{off}}=k_{\mathrm{on}}\cdot k_D$ [see v_2], where k_D is the equilibrium dissociation constant. EpoR is constitutively replenished at the cell surface independently of ligand binding with turnover rate k_t [see v_3 and v_4]. The maximal amount of receptor at the cell membrane is B_{max}. Receptor-ligand complexes are internalized ligand-dependently with rate k_e by endocytosis[14] [see v_5]. The internalized complex can either be recycled back to the plasma membrane or undergo degradation inside the cell. Recycling with rate k_{ex} returns the ligand to the extracellular medium in its active form [see v_6]. Degradation either leaves the ligand inactive inside the cell with rate k_{di} [see v_7] or deposits it to the extracellular medium in its inactive form with rate k_{de} [see v_8]. Initial concentrations are assumed to be zero, except for $[\mathrm{Epo}](t=0)=Epo_0$ and $[\mathrm{EpoR}](t=0)=B_{\mathrm{max}}$ that will be estimated from the experimental data. The reaction fluxes corresponding to each interaction are given by

$$v_1 = k_{\mathrm{on}}\cdot[\mathrm{Epo}]\cdot[\mathrm{EpoR}],$$

$$v_2 = k_{\mathrm{on}}\cdot k_D\cdot[\mathrm{Epo\_EpoR}],$$

$$v_3 = k_t\cdot B_{\mathrm{max}},$$

$$v_4 = k_t\cdot[\mathrm{EpoR}],$$

$$v_5 = k_e\cdot[\mathrm{Epo\_EpoR}],$$

$$v_6 = k_{\mathrm{ex}}\cdot[\mathrm{Epo\_EpoR\_i}],$$

$$v_7 = k_{di}\cdot[\mathrm{Epo\_EpoR\_i}],$$

$$v_8 = k_{de}\cdot[\mathrm{Epo\_EpoR\_i}],$$

and yield with

$$\mathrm{d}/\mathrm{d}t[\mathrm{Epo}] = -v_1+v_2+v_6,$$

$$\mathrm{d}/\mathrm{d}t[\mathrm{EpoR}] = -v_1+v_2+v_3-v_4+v_6,$$

$$\mathrm{d}/\mathrm{d}t[\mathrm{Epo\_EpoR}] = +v_1-v_2-v_5,$$

$$\mathrm{d}/\mathrm{d}t[\mathrm{Epo\_EpoR\_i}] = +v_5-v_6-v_7-v_8,$$

$$\mathrm{d}/\mathrm{d}t[\mathrm{dEpo\_i}] = +v_7,$$

$$\mathrm{d}/\mathrm{d}t[\mathrm{dEpo\_e}] = +v_8,$$

the ODE system describing the time evolution of species concentration.

Experimental technique. By employing radio labeled ligand,[4] the dynamics of Epo concentration can be observed in BaF3-EpoR cells[1] in various compartments of the biological system. The unknown calibration factor *scale* links the activity of ^{125}I given in cpm to concentration scale of Epo given in pM.

Numerical techniques. The ODE systems was solved nu-

Author complimentary copy. Redistribution subject to AIP license or copyright, see http://cha.aip.org/cha/copyright.jsp

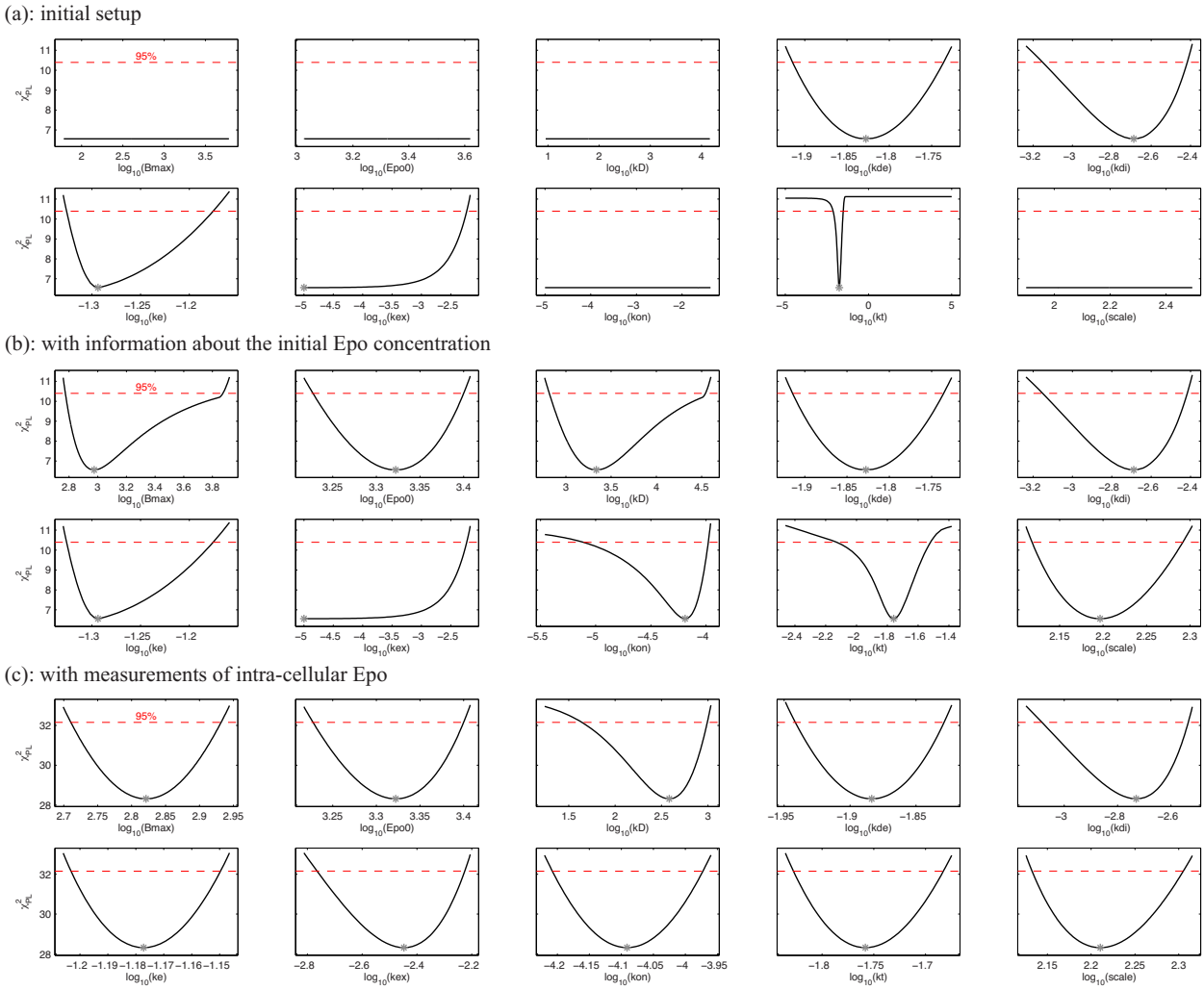

FIG. 3. (Color online) The profile likelihood χ^2_{PL} of the model parameters are displayed in combination with the thresholds $\Delta_{0.95}$ yielding with $df=1$ confidence intervals that hold for each parameter individually. The optimal parameter value is indicated by an asterisk, if unique. (a) The flatness of the profile likelihood reveals that five parameters are structurally nonidentifiable, given the initial setup. (b) By including information about the initial Epo concentration, the structural nonidentifiability can be resolved. Parameter k_{ex} remains practically nonidentifiable. (c) By including measurements of intracellular Epo, all parameters are structurally and practically identifiable.

merically by CVODES.[5] The algorithm simultaneously computes the variational equations.[7] This allows to supply derivatives for the estimation of the parameters by the lsqnonlin-algorithm of MATLAB.[3]

A. Initial setup

In a first experiment, Epo concentration was recorded in triplicates in two compartments: in the extracellular medium (y_1) and bound to EpoR on the cell membrane (y_2),

$$y_1 = scale \cdot ([\mathrm{Epo}] + [\mathrm{dEpo\_e}]),$$

$$y_2 = scale \cdot [\mathrm{Epo\_EpoR}]$$

(see the dashed boxes in Fig. 2). After parameter estimation, a good model to data agreement with a value of the objective function $\chi^2=6.55$ for 16 data points and 10 free parameters is obtained. To investigate the uncertainty in the parameter estimates, the profile likelihood of each parameter was evaluated, as displayed in Fig. 3(a). The calculation takes about 30 s per parameter on a normal office computer.

The flatness of the profile likelihood reveals that parameters $B_{\max}$, Epo_0, k_D, k_{on}, and *scale* are structurally nonidentifiable. The change of the other parameters along the profile likelihood of one of these parameters indicates functional

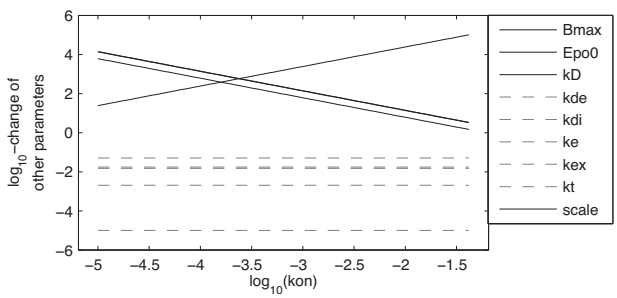

FIG. 4. Initial setup: the change of the other parameters along the profile likelihood $\chi^2_{\mathrm{PL}}(k_{\mathrm{on}})$ indicates functional relations between all five structural nonidentifiable parameter, indicated by the solid lines.

Author complimentary copy. Redistribution subject to AIP license or copyright, see http://cha.aip.org/cha/copyright.jsp

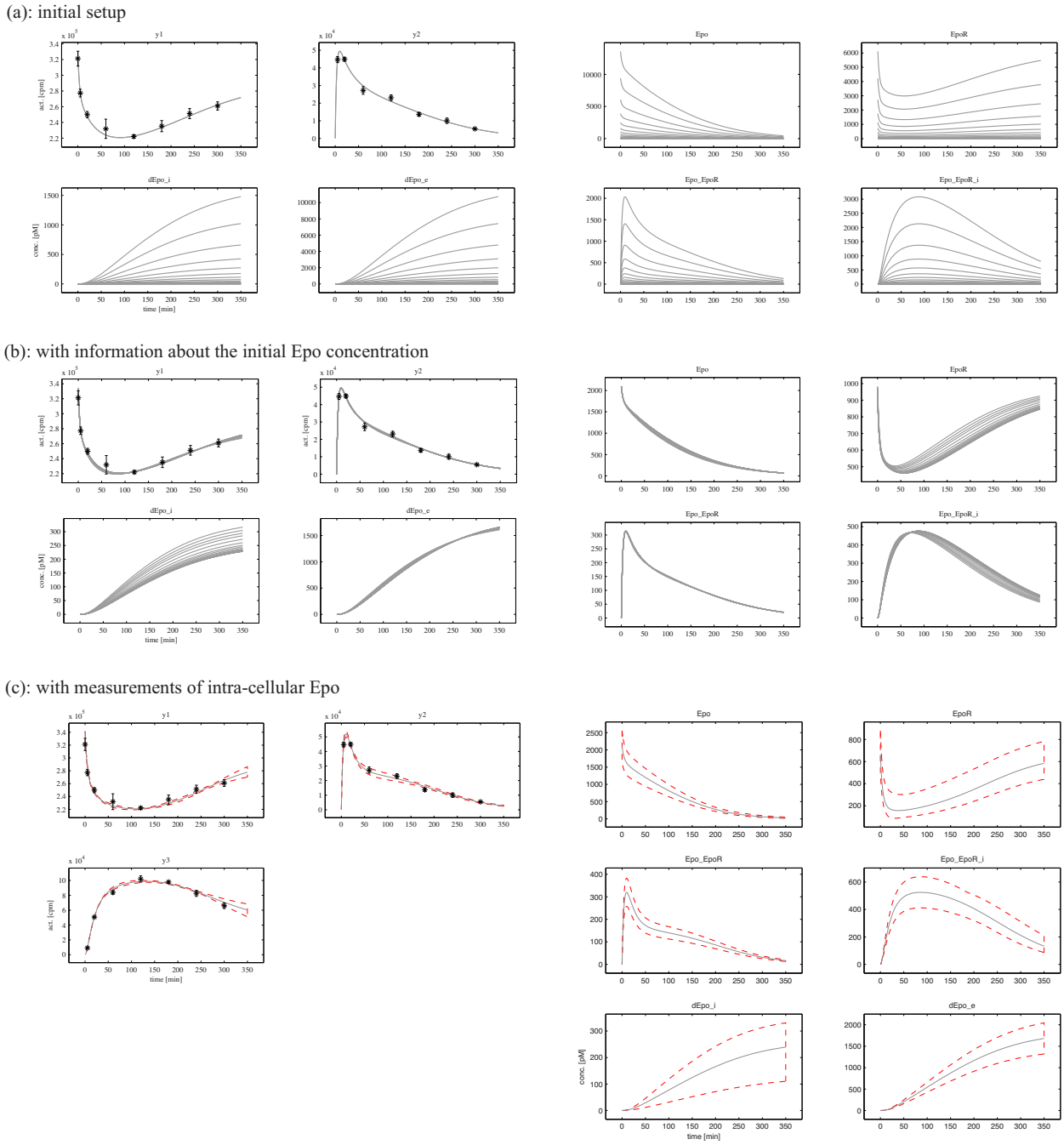

FIG. 5. (Color online) The figure shows dependency of the trajectories of the model observable $\vec{y}$ and of species concentration $\vec{x}$ on uncertainties in the parameter estimates. (a) The concerted change of parameters along the structural nonidentifiability of k_{on} (see Fig. 4) does not affect the model observables but shift the trajectories of species concentration by a common factor. (b) The practical nonidentifiability of k_{ex} only slightly affects the model observables $\vec{y}$, staying in agreement with the measurement precision of the experimental data. Nevertheless, the trajectories of species EpoR, Epo_EpoR_i, and dEpo_i are affected. (c) The remaining uncertainties in the identifiable parameters, as displayed in Fig. 3(c), translate to confidence intervals of the model trajectories.

relations linking the five structural nonidentifiable parameters, see, e.g., for $\chi^2_{PL}(k_{on})$ in Fig. 4. The corresponding effect on the model trajectories of this concerted change in the parameters can be illustrated by plotting the model trajectories for parameter value along the profile likelihood of one of these parameters, see, e.g., for $\chi^2_{PL}(k_{on})$ in Fig. 5(a). As expected, the model observables $\vec{y}$ are not affected, but the trajectories of species concentration $\vec{x}$ are shifted by a common factor. The structural nonidentifiability represents a freedom in the choice of the concentration scale and is a result of missing information about absolute concentration in the experimental setup. Consequently, all parameters containing concentration in their unit are affected. Similar results were obtained in Raue *et al.*[11] for a model published by Swameye *et al.*[13]

B. Including absolute concentrations

In order to resolve the structural nonidentifiability, the observability analysis presented in Fig. 5(a) suggests to in-

Author complimentary copy. Redistribution subject to AIP license or copyright, see http://cha.aip.org/cha/copyright.jsp

TABLE I. Individual confidence intervals $[\sigma^-, \sigma^+]$ of the model parameter to a confidence level of 95%. Values are given on a $\log_{10}$ scale. The CRs of the estimates are in line with the expected values (93.33% and 96.66%).

Name	$\hat{\theta}$	σ^-	σ^+	Unit	CR (%)
B_{max}	+2.821	+2.710	+2.932	pM	95.78
Epo_0	+3.322	+3.227	+3.400	pM	92.44
k_D	+2.583	+1.641	+2.993	pM	95.78
k_{de}	−1.884	−1.941	−1.829	1/min	95.78
k_{di}	−2.730	−3.083	−2.535	1/min	95.56
k_e	−1.177	−1.203	−1.150	1/min	97.33
k_{ex}	−2.447	−2.764	−2.225	1/min	96.44
k_{on}	−4.091	−4.208	−3.973	1/(pM min)	95.56
k_t	−1.758	−1.828	−1.683	1/min	97.33
Scale	+2.210	+2.133	+2.305	cpm/pM	92.89

clude information about the absolute concentration of one of the species. For the experiment, the cells were treated with 2100 ± 210 pM of ^{125}I-Epo. Therefore, a prior distribution of the parameter $Epo_0 \sim N(2100, 210^2)$ is assumed by penalizing the objective function of Eq. (3) with an additional summand $(Epo_0 - 2100)^2/210^2$. Recalculating the profile likelihood verifies that the structural nonidentifiability is resolved [see Fig. 3(b)]. Nevertheless, the parameter k_{ex} remains practically nonidentifiable. Its upper confidence bound is determined at $\sigma^+ = -2.230$ but its lower confidence bound is not feasible.

C. Including measurement of intracellular Epo

In order to efficiently resolve the practical nonidentifiability of k_{ex}, additional measurements need to be planned. Therefore, the variability of the model trajectories along the profile likelihood $\chi^2(k_{ex})$ is investigated, as displayed in Fig. 5(b). The available model observables y_1 and y_2 show only slight variations and hence are not suitable for additional measurements. However, the trajectories of Epo_EpoR_i and dEpo_i show much larger variations and suggest an additional measurement of ^{125}I-Epo inside the cell,

$$y_3 = scale \cdot ([\text{Epo\_EpoR\_i}] + [\text{dEpo\_i}]),$$

which was recorded in triplicates as well. After including the additional data, the profile likelihood of all model parameters indicate their structural and practical identifiability, as displayed in Fig. 3(c).

Confidence intervals. The resulting confidence intervals of the now identifiable parameters are finite and their values are given in Table I. Finally, the remaining uncertainties can be translated to confidence intervals of the model trajectories. Therefore, the trajectories corresponding to all acceptable parameter value according to the profile likelihood are evaluated. The resulting upper and lower confidence bands are displayed in Fig. 5(c) for the threshold $\Delta_{0.95}$ that is also indicated in Fig. 3(c) for the derivation of confidence intervals of the model parameters. Based on a confidence threshold with $df = 1$, the confidence bands have to be interpreted pointwise for each time point individually.

In order to ensure the appropriateness of the derived confidence intervals, we performed a simulation study by assuming that the estimated parameter values given in Table I are the true values. Using these values and the same model outputs, measurement time points and measurement noise as in the original experimental data set, 450 independent data sets were generated. After estimating the parameters for each of these data sets, the resulting distribution of the overfitting is in line with the χ^2_{df}-distribution with $df = 10$, the number of estimated parameters [see Fig. 6(a)]. This verifies that the threshold Δ_α utilized to derive the likelihood-based confidence intervals was assessed correctly.

Coverage rates. In order to compute coverage rates for the parameter estimates, for each of the simulated data sets, 95% individual confidence intervals were calculated. According to the 0.05 and 0.95 quantiles of the binomial distribution, the coverage rates (CRs) for 450 simulated data sets and a 95% confidence level are expected to be between 93.33% and 96.66%. For all parameters, this is fulfilled (see in Table I). Coverage rates can also be assessed for the time pointwise confidence bands on the model trajectories shown in Fig. 5(c) [see Fig. 6(b)]. The coverage rates are, in most

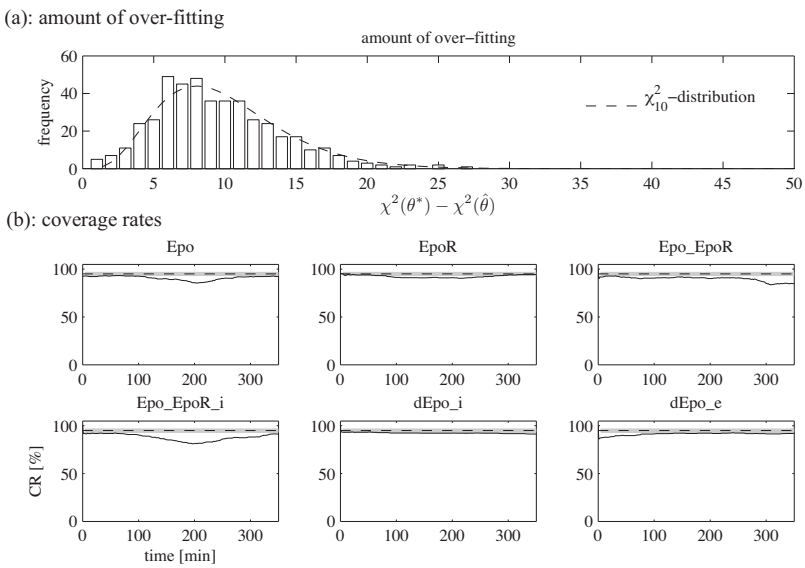

FIG. 6. The appropriateness of confidence intervals was assessed by a simulation study with 450 generated data sets. (a) Comparison of the amount of overfitting to the expected χ^2_{df} distribution with $df = 10$. (b) The solid lines indicate the CRs for the time pointwise confidence bands on the model trajectories shown in Fig. 5(c). The dashed lines are the desired 95% level of confidence, while the gray shades are the expected coverage rates.

Author complimentary copy. Redistribution subject to AIP license or copyright, see http://cha.aip.org/cha/copyright.jsp

cases, in line with their expected values described by the 0.05 and 0.95 quantiles of the binomial distribution. Too low coverage rates are observed for species Epo at $t \approx 20$ min, for Epo_EpoR at $t > 300$ min, and for Epo_EpoR_i between 150 and 250 min. Here, increase attention is indicated when interpreting the results. The deviations occur because the high-dimensional confidence region in parameter space was not sampled densely but approximated by the profile likelihood.

IV. SUMMARY

By using a mathematical model of Epo/EpoR interaction and trafficking, the iterative cycle between modeling and experimentation in systems biology was demonstrated. Based on an initial data set, parameter identifiability and observability was successively improved by applying the profile likelihood approach. This general and efficient approach allows to investigate both the structural and practical identifiability of the model parameters and the observability of model trajectories. The results of the analysis were used to plan additional experiments to resolve nonidentifiabilities inherent in the initial data set. Finally, a fully identifiable model was obtained that allows for reliable prediction of the system dynamics.

ACKNOWLEDGMENTS

We thank Clemens Kreutz, Thomas Maiwald, Julie Bachmann, and Marcel Schilling for their support.

This work was supported by the German Federal Ministry of Education and Research [Virtual Liver, LungSys (Grant No. 0315415E, and FRISYS (Grant No. 0313921)], the European Union [CancerSys (Grant No. EU-FP7 HEALTH-F4-2008-223188], the Initiative and Networking Fund of the Helmholtz Association within the Helmholtz Alliance on Systems Biology (SBCancer DKFZ II.1), and the Excellence Initiative of the German Federal and State Governments (EXC 294).

[1]A cell line of murine bone marrow-derived progenitor B-cells expressing the Epo receptor.
[2]Becker, V., Schilling, M., Bachmann, J., Baumann, U., Raue, A., Maiwald, T., Timmer, J., and Klingmüller, U., "Covering a broad dynamic range: Information processing at the erythropoietin receptor," Science **328**, 1404–1408 (2010).
[3]Coleman, T. and Li, Y., "An interior, trust region approach for nonlinear minimization subject to bounds," SIAM J. Optim. **6**, 418–445 (1996).
[4]Decay of the iodine isotope $^{125}\mathrm{I} \rightarrow {}^{125}\mathrm{Te}$ by electron capture with $T_{1/2} = 59.408$ days and $E_\gamma = 0.186$ MeV.
[5]Hindmarsh, A., Brown, P., Grant, K., Lee, S., Serban, R., Shumaker, D., and Woodward, C., "Sundials: Suite of nonlinear and differential/algebraic equation solvers," ACM Trans. Math. Softw. **31**, 363–396 (2005).
[6]Lehmann, E. and Leo, E., *Theory of Point Estimation* (Wiley, New York, 1983).
[7]Leis, J. and Kramer, M., "The simultaneous solution and sensitivity analysis of systems described by ordinary differential equations," ACM Trans. Math. Softw. **14**, 45–60 (1988).
[8]Meeker, W. and Escobar, L., "Teaching about approximate confidence regions based on maximum likelihood estimation," Am. Stat. **49**, 48–53 (1995).
[9]Murphy, S. and van der Vaart, A., "On profile likelihood," J. Am. Stat. Assoc. **95**, 449–485 (2000).
[10]Press, W., Teukolsky, S., Flannery, B., and Vetterling, W., *Numerical Recipes: FORTRAN* (Cambridge University Press, Cambridge, 1990).
[11]Raue, A., Kreutz, C., Maiwald, T., Bachmann, J., Schilling, M., Klingmuller, U., and Timmer, J., "Structural and practical identifiability analysis of partially observed dynamical models by exploiting the profile likelihood," Bioinformatics **25**, 1923–1929 (2009).
[12]Seber, G. and Wild, C., *Nonlinear Regression* (Wiley, New York, 2003).
[13]Swameye, I., Müller, T., Timmer, J., Sandra, O., and Klingmüller, U., "Identification of nucleocytoplasmic cycling as a remote sensor in cellular signaling by data based modeling," Proc. Natl. Acad. Sci. U.S.A. **100**, 1028–1033 (2003).
[14]The taking in of matter by engulfment with the cell membrane.
[15]Timmer, J., Müller, T., Swameye, I., Sandra, O., and Klingmüller, U., "Modeling the nonlinear dynamics of cellular signal transduction," Int. J. Bifurcation Chaos Appl. Sci. Eng. **14**, 2069–2079 (2004).
[16]Venzon, D. and Moolgavkar, S., "A method for computing profile-likelihood-based confidence intervals," Appl. Stat. **37**, 87–94 (1988).
[17]Walter, E., *Identifiability of Parametric Models* (Pergamon, New York, 1987).

Author complimentary copy. Redistribution subject to AIP license or copyright, see http://cha.aip.org/cha/copyright.jsp